Robot Path Planning Method Combining Enhanced APF and Improved ACO Algorithm for Power Emergency Maintenance

Wei Wang, Maintenance Branch, State Grid Shanxi Electric Power Company, China*

Xiaohai Yin, Maintenance Branch, State Grid Shanxi Electric Power Company, China

Shiguang Wang, Maintenance Branch, State Grid Shanxi Electric Power Company, China

Jianmin Wang, Maintenance Branch, State Grid Shanxi Electric Power Company, China

Guowei Wen, Maintenance Branch, State Grid Shanxi Electric Power Company, China

ABSTRACT

Considering the limited adaptability of the existing substation inspection robot path planning (PP) algorithms, the authors propose a novel PP method for mobile robots (MR) based on the structure of the ultra-high voltage (UHV) substation inspection robot system. The proposed method combines the improved ant colony optimization (IACO) algorithm and the enhanced artificial potential field (EAPF) algorithm. To minimize the interference of the pheromones, they introduced a pheromone adjustment coefficient in the later iterations of the algorithm. Furthermore, they improved the global pheromone update method, which is beneficial to the MR to search for the optimal path (OP) rapidly. They constructed two environmental models using the grid method, and they used MATLAB to implement comparative experiments between the proposed algorithm and other advanced methods. The results demonstrate that the proposed algorithm outperforms other methods in terms of running time, convergence speed, and global optimization ability.

KEYWORDS

Enhanced Artificial Potential Field, Improved Ant Colony Optimization, Inspection Robot, Path Planning, UHV Substation

INTRODUCTION

Substations, as an essential part of the power grid, play a vital role in ensuring the safe operation of the entire power grid. Hence, substation inspections serve as the basis for the reliable operation of the substation equipment (Wang et al., 2019). With the massive deployment and development of ultra-high voltage (UHV) AC and DC projects, conventional inspection methods are no longer suitable for the large-scale area and multidevice characteristics of UHV substations. The application of

automatic inspection robots in substations will guarantee efficiency and safety, addressing some of the shortcomings of traditional manual inspections (Zhao et al., 2022). Path planning (PP) is one of the key techniques of inspection robots, and the research has important practical significance (Shiling, 2020). An intelligent robot is a kind of mechanical technology invented and developed based on computer technology (Wang et al., 2018). Intelligent robots are based on the design principles of intelligent robots in power equipment, and their main structure includes four components: a human-computer interaction system, a control system, a navigation system, and a sensor system (Ding et al., 2018). The intelligent robot can effectively realize the overhaul and power equipment fault diagnosis and achieve better power operation and maintenance performance through the interaction and cooperation of these four major components. Moreover, intelligent robots can consciously perceive the operating conditions of surrounding equipment through the acceleration and infrared sensors within the sensing system and convey real-time operating environment-related information to the power equipment operators in time (Alaraifi et al., 2013).

The ant colony optimization (ACO) algorithm is a self-heuristic and swarm intelligence method. It is not subject to external interference, adapts to complex and changeable environments, and is very robust (Wu et al., 2018). Based on these advantages, the ACO algorithm is chosen for PP tasks. However, this algorithm has limitations, such as being easily trapped in the local optimum issue, long optimization time, and slow optimization speed. To address these issues, we propose a mobile robot path planning (MRPP) method that combines the enhanced artificial potential field algorithm (EAPF) and the improved ant colony optimization algorithm (IACO), applied to the PP tasks of the inspection robots in the UHV substation environment. We used the grid method to build the working environment of the UHV substation for simulation, and the simulation results further verified the superiority of the proposed method.

RELATED WORKS

Nowadays, many intelligent algorithms have been applied to the MRPP, such as the D* algorithm, ACO algorithm, APF method, and artificial fish swarm algorithm (Ab Wahab et al., 2020). Each of these algorithms has its own advantages and drawbacks. The advantages of different algorithms are combined to provide new methods for solving MRPP, such as the combination of the APF method and ACO algorithm (Wang et al., 2018) or the fusion of the particle swarm algorithm and the A* algorithm (Lian et al., 2020).

The APF method is comprehensively adopted in robot PP owing to its small computation requirements, simple structure, and smooth path (Azzabi & Nouri, 2019). However, the APF method is susceptible to local minimum points, where the MR may become a stationary state or oscillate within a certain range in front of an obstacle owing to the force balance problem, resulting in a failure to reach the target point. To solve this problem, various researchers have proposed different solutions. Zhang et al. (2018) added a chaos optimization algorithm to the APF method using the potential field function as the objective function for chaos optimization and determining the associated moving step size and direction of the MR through chaos search. Orozco-Rosas et al. (2019) investigated a new repulsion potential field function to eliminate local minima and employed the quantum genetic algorithm to select the optimal or suboptimal individual for path optimization. Wang et al. (2021) proposed combining the artificial potential field (APF) method with fuzzy control; these researchers then adopted a particle swarm-based algorithm to optimize the membership function of the fuzzy logic controller. This approach was applied to the motion control of MR, overcoming the local minimum problem. However, most of these aforementioned methods are suitable only for simple environments.

As a heuristic searching algorithm, the ACO algorithm is developed by simulating the food-finding behavior of ants in the wild. It embodies the internal features of positive feedback, parallelized computation, and descent robustness (Gao et al., 2020), making it a popular choice for robot PP tasks. Jiao et al. (2018) proposed a polymorphic ACO algorithm for PP using the adaptive state transition

and adaptive updating strategies to guarantee the corresponding importance of the strengths of pheromones and heuristic information in the repeated cycles of the algorithm. However, this method has a relatively small search space and a weak exploration ability. Wang et al. (2017), divided the PP process into two steps: First, the genetic algorithm was used to obtain the initial path, and then the optimal paths were regarded as the reference for performing the initialization of pheromones for the ACO algorithm, alleviating the mindlessness in the initial searching process of the ACO algorithm. The ACO was then designed to make further steps in optimizing the initial path. Results indicated that the algorithm can avoid local optima and achieve a fast convergence speed. Wang et al. (2018) presented an MRPP method combining the improved ACO with potential field heuristic information. These researchers constructed comprehensive heuristic information using the APF method and introduced a decline coefficient to avoid local optima. Results have proven the effectiveness and feasibility of this method.

Many studies have been conducted on technologies related to PP tasks with inspection robots in UHV substations. Zhang et al. (2019) proposed combining a heuristic searching algorithm with an improved Dijkstra method to perform PP of MR in the substation scenes, considering the real-world system operation condition and using the times and angles of each turning as evaluating metrics. Chen et al. (2019) analyzed the PP problem in the presence of sophisticated substation scenes and validated a PP method for several MRs as well as a time-window-based solution. Results indicated that the solution can be effective and feasible in avoiding different categories of conflicts in the PP process. However, these methods still face challenges such as high algorithm complexity, high memory overhead, and poor real-time performance.

In the rest of this paper, we introduce the structure of the electric power inspection robot system, explain the EAPF method, propose an improved ACO algorithm fused with the EAPF method, present the experimental results and analysis, and share our conclusions.

SYSTEM ARCHITECTURE

The structure of the robot inspection system is shown in Figure 1. It consists of two main parts: the host computer system and the MR. The host computer system includes a background monitoring system, background industrial computer, remote robot operation, image processing, positioning system, inspection report generation and query, industrial wireless network, and other components. The host computer system is responsible for receiving, recording, and processing image information obtained from the MR. The robot body comprises an embedded main controller, a digital signal processor (DSP) executor, a task controller, sensor modules, image acquisition modules, and wireless communication modules. These components are responsible for collecting on-site image information and sending it to the host computer system using wireless communication, thereby reducing the workload of substation employees.

Consequently, the robot can perform broad inspection coverage of the equipment on the site by receiving the work instructions sent by the system and executing the corresponding work tasks. Through the application of an intelligent system, the functions of independent inspection, remote operation, online detection, and intelligent alarm are realized, helping users achieve unattended and improve the intelligent operation and maintenance of substations.
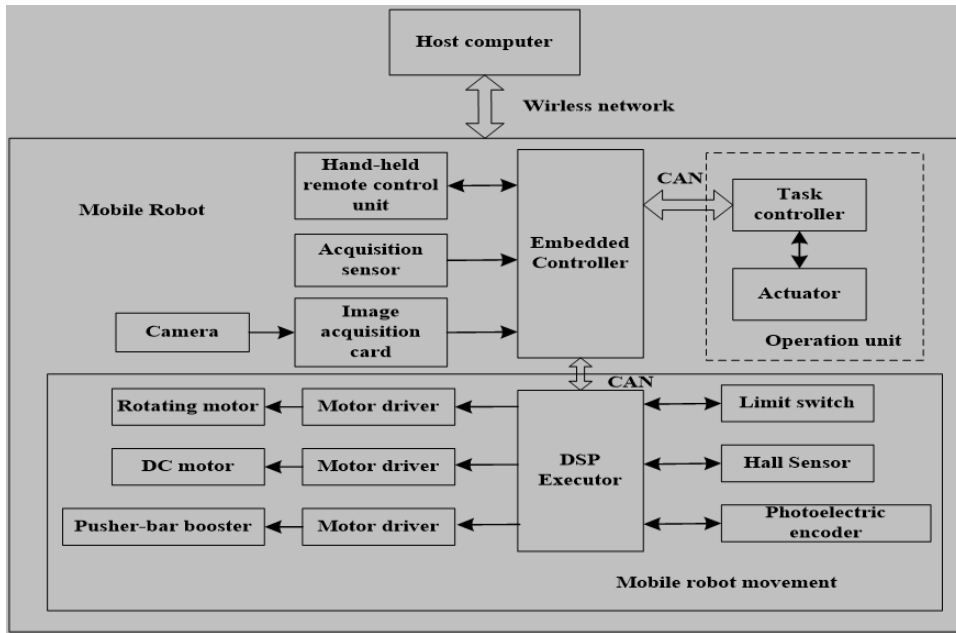
APF METHOD

In this section we discuss our experiment with the APF method.

Enhanced APF Method

We combined the enhanced APF with the improved ACO algorithm.

Figure 1. Robot inspection system structure

Distance Detection and Threshold Establishment

The function of the gravitational field is formally defined as shown in equation (1).

$$U_a = \frac{1}{2}k(x_g - x)^2 \tag{1}$$

In this equation, U_a denotes the function of the gravitational potential field, $k > 0$ indicates the gravitational field coefficient, and x_g represents the coordinate for the targeted point.

The repulsion field function is defined as shown in equation (2).

$$U_r = \begin{cases} \frac{1}{2}m(\frac{1}{\rho} - \frac{1}{P_0})^2 & \rho \le P_0 \\ 0 & \rho > P_0 \end{cases} \tag{2}$$

In equation (2), $m > 0$ denotes the repulsion field coefficient, P_0 symbolizes the influencing radius of the obstacle, representing the shortest distance between the robot and the obstacle. The obstacle will initiate a repulsive force on the robot if—and only if—the distance from the robot to the obstacle is less than P_0.

When the robot becomes trapped in a local minimum, the robot will stay at a certain point or move back and forth within a small range. According to this feature, the unit time is used to detect the robot's moving distance, and the detected distance is compared with a preset threshold. If the moving distance per unit of time is less than the threshold, it is determined that the robot has fallen into a local minimum.

Virtual Traction

If the robot enters the U-shaped area composed of obstacles and becomes trapped in a local minimum problem, as shown in Figure 2, the current coordinates of the robot and the obstacle located at the outermost end of the U-shaped area are calculated.

Given an influencing length of the obstacle, denoted as r, the obstacle is converted into a circle with a radius of r, and the coordinate of the tangent point between the robot and the circle is calculated. Subsequently, a virtual traction point is generated along the line from the robot to the tangent point at a distance d from the tangent point. The traction force will then affect the robot, moving it toward the virtual traction point. Once the robot reaches the virtual traction point, the traction point disappears, and the gravitational force received by the robot automatically switches to the force from the original target point. Suppose the robot encounters the local minimum point again during the robot's operation. In that case, the threshold is compared according to the previous rule and then automatically switches to the virtual traction point rules to facilitate the robot's escape from the local minimum point.

The modeling method for setting the virtual traction point is as follows: Let (x_0, y_0) denote the current coordinates of the robot and (a_1, a_2) represent the coordinate of the obstacle. The tangent point coordinates are (x_1, y_1), and the coordinates of the virtual traction point are (x, y). First, the distance between the robot to the obstacle is calculated as shown in equation (3).

$$l = \sqrt{(a_1 - x_0)^2 + (a_2 - y_0)^2} \tag{3}$$

In Figure 2, the angles are $\alpha = \arcsin(r / l)$ and $\gamma = \arctan \frac{a_1 - x_0}{a_2 - y_0}$. The length from the robot to the tangent point is obtained by $s = \sqrt{l^2 - r^2}$. Thus, the coordinates of the tangent point can be obtained as shown in equation (4).

$$\begin{cases} x_1 = x_0 - \sin \beta \times s \\ y_1 = y_0 - \cos \beta \times s \end{cases} \tag{4}$$

Figure 2. Force analysis for the robot in local minimum
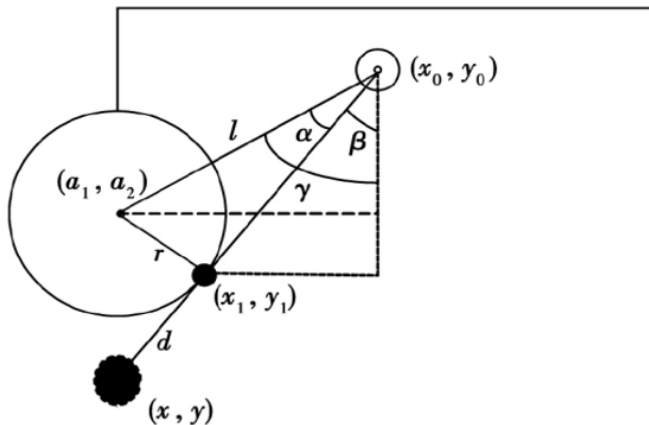
Substitute the parameters yields as shown in equation (5).

$$\begin{cases} x_1 = x_0 - \sin(\arctan\dfrac{a_1 - x_0}{a_2 - y_0} - \arcsin\dfrac{r}{l}) \times \sqrt{(a_1 - x_0)^2 + (a_2 - y_0)^2 - r^2} \\ y_1 = y_0 - \cos(\arctan\dfrac{a_1 - x_0}{a_2 - y_0} - \arcsin\dfrac{r}{l}) \times \sqrt{(a_1 - x_0)^2 + (a_2 - y_0)^2 - r^2} \end{cases} \tag{5}$$

Based on the tangent coordinates (x_1, y_1) and the robot coordinates (x_0, y_0), the formulas shown in equations (6) and (7) can be established.

$$(y - y_1) / (x - x_1) = -(x_0 - x_1) / (y_0 - y_1) \tag{6}$$

$$d^2 = (x - x_1)^2 y + (y - y_1)^2 \tag{7}$$

The final virtual traction point coordinates (x, y) can be calculated as shown in equation (8).

$$\begin{cases} x = x_1 \pm \dfrac{d(x_0 - y_1)}{\sqrt{(x_0 - x_1)^2 + (y_0 - y_1)^2}} \\ x = y_1 \pm \dfrac{d(x_0 - y_1)}{\sqrt{(x_0 - x_1)^2 + (y_0 - y_1)^2}} \end{cases} \tag{8}$$

Speed-Up Function

The gravitational force generated by the virtual traction point is given by equation (9).

$$\boldsymbol{F}_\iota = -k(x - x_0) \tag{9}$$

During movement, the robot is subjected to the virtual traction force, generating acceleration ι to move toward the virtual traction point. However, the traction force $\boldsymbol{F}_\iota$ is limited. To increase acceleration and improve efficiency, the virtual traction force is rapidly increased in a short period to maintain system stability during movement. The exponential function with a coefficient greater than 1 can increase rapidly in a relatively short period. To leverage this property, an exponential function item is added in the modeling to increase the virtual traction as shown in equations (10) and (11).

$$\boldsymbol{F}_\iota = k\left[(x_0 - x) + \iota_1^{(c-d)}\right] \times f(t) \tag{10}$$

$$f(t) = \begin{cases} 1, \nabla l \le S \\ 0, \nabla l > S \end{cases} \tag{11}$$

In these equations, $\boldsymbol{F}_t$ symbolizes the traction force generated by the virtual traction point, $f(t)$ denotes the switch function, and ∇l defines the moving distance of the robot per unit of time. In addition, S indicates the preset threshold, c represents the coordinates of the virtual traction point obtained using equation (8), ι_1 represents an exponential function coefficient greater than 1, and d shows the robot position coordinates.

IMPROVED ACO COMBINED WITH ENHANCED APF

Now we discuss steps we took to combine the ACO with the enhanced APF.

Heuristic Function for the Force of the Potential Field

The heuristic function constructed by the original ACO algorithm calculates only the distance between nodes (Dai et al., 2019). In this case, d_{ij} represents the Euclidean distance from the current node position i to the reachable node j in the next step, as shown in equation (12). The ant k at node i selects node j as the next position to reach, and the position selection probability is calculated by equation (13), where m_k denotes a position set that ant k can choose to reach in the next step, τ_{ij} represents the pheromone value of the path (i, j), η_{ij} indicates the heuristic function, α denotes pheromone heuristic factor, and β defines the weighting parameter for function η_{ij}. The smaller the d_{ij}, the larger the heuristic function, resulting in a greater probability that node i will choose node j.

$$\eta_{ij} = \frac{1}{d_{ij}} \tag{12}$$

$$p_{ji}^k(t) = \begin{cases} \dfrac{[\tau_{ij}(t)]^\alpha \cdot [\eta_{ij}(t)]^\beta}{\sum\limits_{s \subset m_k} [\tau_{is}(t)]^\alpha \cdot [\eta_{is}(t)]^\beta} & j \in m_k \\ 0 & \text{else} \end{cases} \tag{13}$$

According to equation (13), the heuristic function of the original ACO algorithm is related to only the distance between the current MR position and the position of the next node. Suppose many obstacles are in the vicinity of the endpoint. In that case, the heuristic function of the original ACO may not fully consider the impacting factors, leading to the local optimum problem. Hence, owing to the characteristics of positive feedback from the ACO algorithm, if the initial generation of ants fails to obtain the optimal path (OP) and the ant colony secretes a large number of pheromones, other ants choose this path, resulting in a longer path or even a wrong path.

To tackle the existing limitation of the original ACO algorithm, we initially modified the heuristic function using the length information from the current node to the endpoint, which is calculated with the proposed APF method. Then, to avoid falling into the local optimum and mitigate the impact of the heuristic function on the path searching of the MR, we designed a descending parameter φ within the heuristic function. As the MR approaches the endpoint, the heuristic function plays a smaller role. In addition to considering the distance heuristic information, when the MR encounters a complex environment with multiple obstacles in the path search, it must avoid the obstacles and search for the OP simultaneously. Therefore, the potential field heuristic information should also be taken into account.

The improved heuristic function can be expressed as shown in equation (14).

$$\eta_{ij}(t) = \frac{1-\varphi}{\varphi} \cdot \eta_F(t) \cdot \eta_d(t) \tag{14}$$

In this equation, $\eta_F(t)$ represents the potential heuristic function, $\eta_d(t)$ denotes the length heuristic function, and φ symbolizes a constant greater than 0 and less than 1. To ensure that the MR searches for the shortest path, the algorithm will prioritize to the nodes closer to the targeted point among the available nodes. The length d_{je} from node j to target point e, to be chosen in the next step, will be substituted for the d_{ij} in the original ACO algorithm. The improved distance heuristic function can be expressed as shown in equation (15).

$$\eta_d(t) = \frac{1}{d_{je}} \tag{15}$$

Thus, the potential heuristic function is given as shown in equation (16).

$$\eta_F(t) = \delta^{F_t \cdot \cos\theta} \tag{16}$$

In this equation, δ defines a constant greater than 0 and θ represents the angle between the direction of the MR at the current position i pointing to the next node j and the direction of the resultant force of the potential field F_t. Applying the APF force, the MR is guided to keep away from the obstacles and go toward the endpoint. This approach effectively enhances the convergence speed of the algorithm.

Pheromone Updating Strategy

The pheromones are evenly distributed during the ant colony's initialization in the original ACO algorithm. In the early stage of PP, the pheromone value of each grid position has little difference, leading to the blind search of the MR. In this paper we propose an uneven distribution method of pheromones to increase the pheromone concentration in the relevant area from the starting point to the ending point. The pheromone concentration gradually decays along the direction perpendicular to the start point of the MR to the endpoint.

Equation (17) is a linear function expression connecting the initial point of the MR to the targeted point:

$$y = -x + C \tag{17}$$

In equation (17), C denotes a positive integer. When the line encounters an obstacle, the pheromone concentration value of the grid position where the obstacle location is found is set to zero. The initial pheromone distribution is given by the formula shown in equation (18).

$$
\tau_0 = \begin{cases} T, & y = -x + C \\ \dfrac{C-1}{C} \cdot T, & y = -x + C \pm 1 \\ \dfrac{C-2}{C} \cdot T, & y = -x + C \pm 1 \\ ... \\ \dfrac{1}{C} \cdot T, & y = -x + C \ \text{or} \ y = -x + 2C - 1 \end{cases} \tag{18}
$$

In the coordinate system, the initial pheromone concentration value of the straight line $y = -x + C$ passing through all non-obstacle grids is set to T, which serves as the adjustment parameter of the initial pheromones. Differential allocation of initial pheromones has a significant effect on promoting the convergence speed of the algorithm.

Upon completion of the MR's the movement from node i to node j, the local pheromones of the walking path of the MR must be updated. The update rule for the local pheromones is expressed as shown in equation (19).

$$
\tau_{ij} = (1 - \rho)\tau_{ij} + \omega \cdot \tau_0 \tag{19}
$$

In this equation, ω indicates a parameter within the range of $(0, 1)$; ρ represents the pheromone volatilization coefficient, $\rho \in (0,1)$; and τ_0 denotes the initial value of the pheromone. During the path search process, each time the MR passes through the path (i, j), the local pheromone is updated according to equation (19). After the MR completes a path iteration, the pheromones on all paths are updated step by step. The global pheromone update strategy of the ant system can be expressed as shown in equations (20) and (21).

$$
\tau_{ij}(t + 1) = (1 - \rho) \cdot \tau_{ij}(t) + \Delta\tau_{ij}^{bs}(t) \tag{20}
$$

$$
\Delta\tau_{ij}^{bs} = \begin{cases} \dfrac{1}{L^{bs}}, & \text{path}(i, j) \text{is within the optimal path} \\ 0, & \text{otherwise} \end{cases} \tag{21}
$$

As the number of iterations increases, the positive feedback effect of the ACO algorithm may cause the pheromones to concentrate on the nonoptimal path, leading the MR to prefer paths with higher pheromones. This situation may result in the algorithm converging to a nonoptimal solution. To address this problem and reduce the pheromone interference, the pheromone adjustment coefficient is introduced, and the improved global pheromone update method is given as shown in equation (22).

$$
\tau_{ij}(t + 1) = (1 - e^{(N_k - N_{\max})/N_{\max}}) \cdot ((1 - \rho) \cdot \tau_{ij}(t) + \Delta\tau_{ij}^{bs}(t)) \tag{22}
$$

In this equation, e represents a constant. To prevent the algorithm from converging to a nonoptimal solution, the pheromone adjustment coefficient gradually decreases when N_k increases.

Implementation Details

The proposed EAPF-IACO method can be implemented using the following steps:

Step 1: Initialize all the algorithm parameters, establish a grid map environment, set the initial point and end point of the ant colony, and perform uneven pheromone distribution based on equation (18).

Step 2: Conduct the path search from the starting point with m ants.

Step 3: Substitute the constructed potential field force heuristic function formula from equation (14) and the redesigned pheromone update strategy from equation (22) into the state transition probability in equation (13) and select the node positions to be reached by the ants.

Step 4: Check whether all ants avoid obstacles to reach the end position. If so, store the generated OP in this iteration. Otherwise, return to step 3.

Step 5: Update the pheromone concentration value for each path and the potential field force heuristic function according to equation (14).

Step 6: Determine whether all iterations are completed. If the maximum number of iterations is reached, store and output the OP. Otherwise, return to step 2.

SIMULATION RESULTS AND ANALYSIS

In this section we discuss our analysis of our proposed method in simple and complex environments.

Simulation Parameters

We verified the proposed method's superiority through experimental analysis. We executed the simulation on a computer configured with an Intel i5 processor, 16 GB of memory, and a Windows 10 operating system. The simulation was conducted with MATLAB 2018a software.

In the specific parameters of the algorithm, ρ represents the pheromone evaporating coefficient, and its value range is (0, 1). In this experiment, ρ was set to 0.6, and K was 100, indicating that the algorithm ends after 100 iterations and the number of ants is 100. Within a certain numerical range, increasing the number of ants can lead to a more stable planned path and faster convergence speed.

Given the complexity of real-world substation environments, especially in temporary maintenance, the simulation test environment should be appropriately modified based on the existing grid graph to increase the complexity of the environment as much as possible, making the algorithm more practical. Two simulation environments are established in MATLAB, as shown in Figure 3, where the lower right grid represents the starting point of the robot, and the upper left grid depicts the target point.

Comparison of Experimental Results in a Simple Environment

In a simple simulation environment, the characteristics of each algorithm can be observed from the experimental results owing to fewer obstacles. In the simple simulation environment illustrated in Figure 3(a), the results of the three algorithms are presented in Figures 4 and 5.

Figures 4 and 5 show that the original ACO algorithm falls into a locally optimal solution during the search process primarily because of the ants being misled by the heuristic information while avoiding the first convex obstacle, causing them to choose the right node with a smaller Euclidean distance from the target point. Thereafter, under the effect of positive feedback, the searched path consistently converges to the local solution. The method presented by Wang et al. (2018) and our algorithm proposed in this paper have both modified the heuristic information of the ant colony, thereby avoiding this problem. At the same time, because the APF algorithm provides the correct initial heuristic information for the ant colony, the ant colony acquires a better initial path, thus
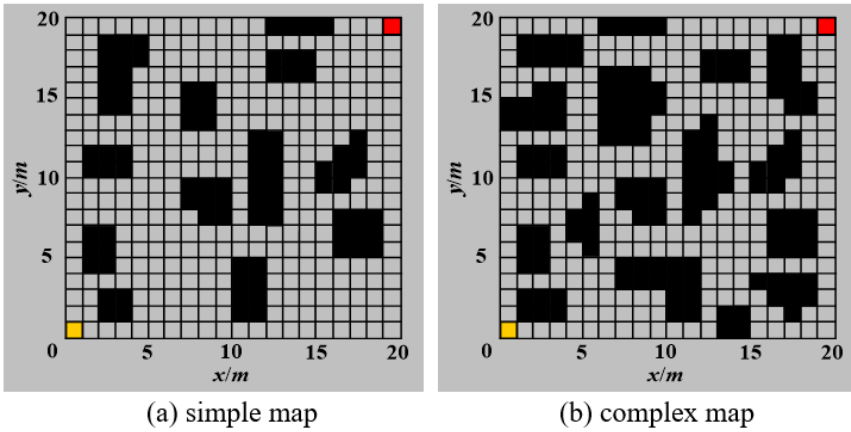
Figure 3. Simulation environment

(a) simple map   (b) complex map

Figure 4. PP results in simple environment

(a) Original ACO

(b) Method proposed
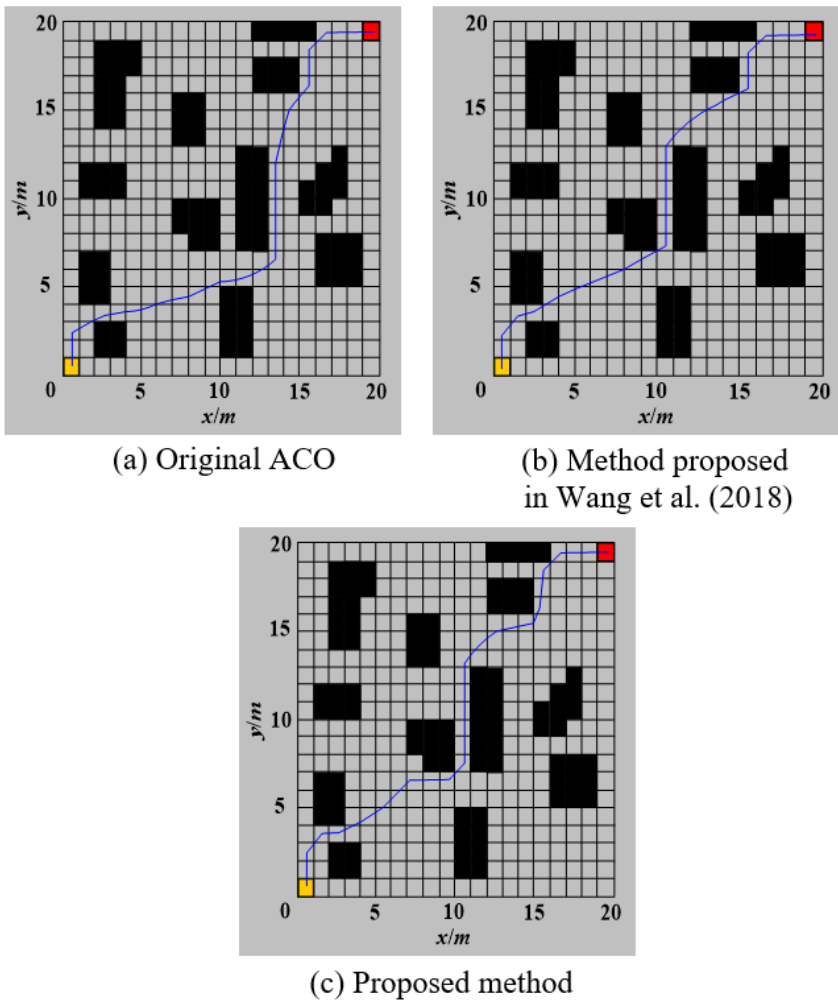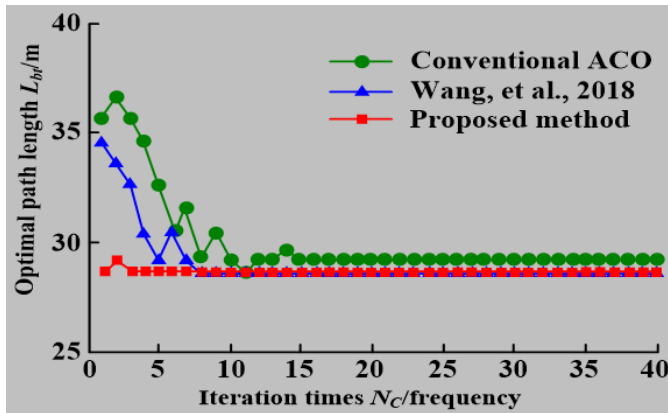in Wang et al. (2018)

(c) Proposed method

Figure 5. Convergence curves in simple environment

enhancing the convergence speed. Nonetheless, Wang et al. (2018) used the original APF algorithm to construct heuristic information, resulting in a significant difference between the initial path and the OP, affecting the subsequent convergence speed of the algorithm. In contrast, our proposed method uses an improved APF algorithm to obtain a superior initial path, greatly improving the convergence speed of the algorithm.

As shown in Figure 4, the path found by the proposed EAPF algorithm is just the OP in a simple environment, leading the IACO algorithm to converge to the optimum after only four iterations. As listed in Table 1, in a simpler scenario, the proposed algorithm has a higher convergence rate and the shortest running time, 0.985 s, compared with the other two algorithms.

Comparison of Experimental Results in a Complex Environment

In a complex environment, as shown in Figure 3(b), simulation experiments were conducted using three different algorithms. The results are shown in Figures 6 and 7.

The results in Figures 6 and 7 demonstrate that the path planned by the original ACO algorithm was still trapped in a local optimum in a complex environment. The OP planned by the proposed method and by Wang et al. (2018) were the same, both being 30.750 m. However, because the proposed method used an EAPF algorithm to inspire the performed search by the ant colony, the initial path was significantly better than that of Wang et al. (2018). The length of the initial path found by the proposed method was 37.657 m, whereas the method proposed by Wang et al. (2018) was 41.174 m.

Moreover, the convergence curve of the algorithm had a certain level of volatility owing to the alternating effects of global pheromones and local pheromones during the iterative courses of the algorithm. These effects seriously affected the converging speed of the algorithm. However, the proposed method effectively reduced the volatility in the iterative process, stabilized the convergence process, and improved the convergence speed of the algorithm. It is worth noting that the proposed method needed only seven iterations to converge to the best solution, whereas the method proposed

Table 1. Simulation results in simple environment

Method	OP Length	Iteration Times	Time
Original ACO	30.789 m	16	2.895 s
Wang et al. (2018)	29.015 m	9	2.275 s
Proposed method	28.429 m	4	0.985 s

Figure 6. PP results in complex environment

(a) Original ACO   (b) Method in Wang et al. (2018)
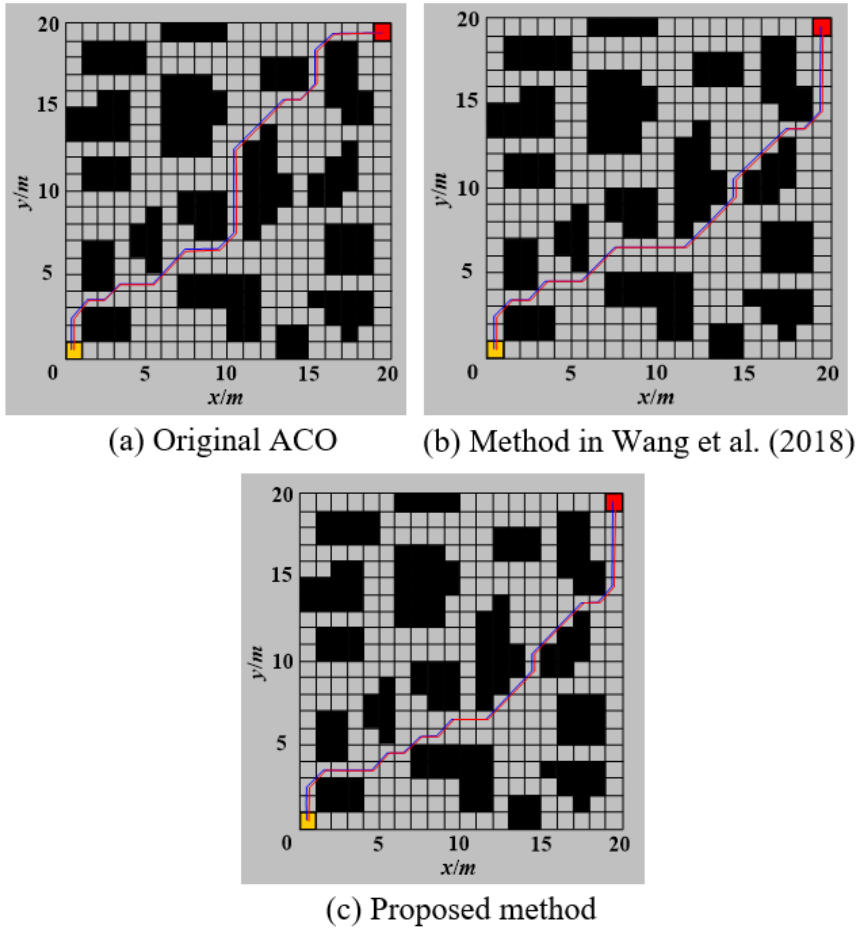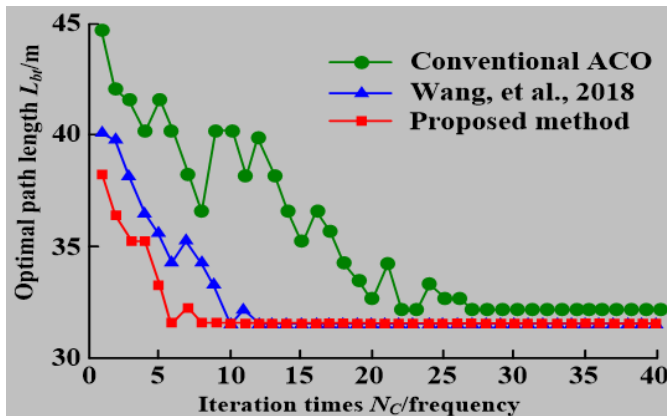
(c) Proposed method

Figure 7. Convergence curves in complex environment

by Wang et al. (2018) required 10 iteration times to converge to the best solution, and the original ACO required at least 25 iteration times to converge.

Furthermore, as shown in Table 2, the proposed method for optimal PP had a significantly shorter operation time than the other two algorithms. The reason is the lower number of iterations for the proposed method and the exclusion of calculations related to invalid obstacles and repulsive force fields in the EAPF algorithm. Thus, the proposed method effectively reduced the computation burdens and shortened the processing time.

Summary of Experimental Results Under Two Different Environments

The simple simulation environment had just a few obstacles, but the original ACO fell into the local best solution in the search process. In contrast, the method presented by Wang et al. (2018) and the proposed algorithm avoided local optimization owing to the improvements in the heuristic information of the ants. In addition, the proposed algorithm incorporated an EAPF algorithm to improve the optimality of the initial path and accelerate the convergence speed. Table 1 indicates that the proposed algorithm had the least number of iterations and the shortest running time compared with other methods. Moreover, it is worth mentioning that the difference in the generated OP lengths by three algorithms was very small owing to the simple characteristics of the simulation environment. However, in the complex simulation environment, the number of iterations and operation times of all the three algorithms were increased significantly. However, the proposed algorithm still maintained the best performance among the comparison methods, as the proposed algorithm can effectively reduce the volatility in the iterative process of the algorithm and stabilize the converging process of the algorithm. In addition, the OP generated by the original ACO was the longest among the comparison methods owing to repeatedly falling into local optima.

CONCLUSION

This paper proposed a PP method for the UHV substation inspection robot based on the EAPF algorithm and the IACO algorithm to enable the UHV substation inspection robot to perform the inspection task quickly and effectively. The novelties of the proposed method based on the EAPF algorithm are listed as follows: the resultant force of the APF was introduced as part of the heuristic information of the path points in the ant colony optimization algorithm, and the heuristic function of the APF forces was constructed, thereby improving the algorithm's convergence speed. Furthermore, an improved global pheromone update method was proposed, so the mobile robot could quickly search for the OP. Simulation experiments were conducted in a grid environment. The results showed that compared with the original ACO algorithm and the method presented by Wang et al. (2018), the proposed method had obvious improvements in terms of the number of iterations, the OP length, and the processing time in the 20×20 grid environment with different complexities.

Table 2. Simulation results in complex environment

Method	OP Length	Iteration Times	Time
Original ACO	35.624 m	25	15.607 s
Wang et al. (2018)	30.750 m	10	7.168 s
Proposed method	30.750 m	7	2.996 s

DATA AVAILABILITY

The data used to support the findings of this study are included within the article.

CONFLICTS OF INTEREST

We declare that there is no conflict of interest regarding the publication of this paper.

FUNDING STATEMENT

REFERENCES

Ab Wahab, M. N., Nefti-Meziani, S., & Atyabi, A. (2020). A comparative review on mobile robot path planning: Classical or meta-heuristic methods? *Annual Reviews in Control*, *50*, 233–252. doi:10.1016/j.arcontrol.2020.10.001

Alaraifi, A., Molla, A., & Deng, H. (2013). An empirical analysis of antecedents to the assimilation of sensor information systems in data centers. *International Journal of Information Technologies and Systems Approach*, *6*(1), 57–77. doi:10.4018/jitsa.2013010104

Azzabi, A., & Nouri, K. (2019). An advanced potential field method proposed for mobile robot path planning. *Transactions of the Institute of Measurement and Control*, *41*(11), 3132–3144. doi:10.1177/0142331218824393

Chen, X., Zhang, X., Huang, W., Liu, S., & Dai, S. (2019). Coordinated optimal path planning of multiple substation inspection robots based on conflict detection. In *Proceedings of the 2019 Chinese Automation Congress (CAC)* (pp. 5069-5074). IEEE. doi:10.1109/CAC48633.2019.8996479

Dai, X., Long, S., Zhang, Z., & Gong, D. (2019). Mobile robot path planning based on ant colony algorithm with A* heuristic method. *Frontiers in Neurorobotics*, *13*, 15. doi:10.3389/fnbot.2019.00015 PMID:31057388

Ding, I.-J., Lin, R.-Z., & Lin, Z.-Y. (2018). Service robot system with integration of wearable Myo armband for specialized hand gesture human–computer interfaces for people with disabilities with mobility problems. *Computers & Electrical Engineering*, *69*, 815–827. doi:10.1016/j.compeleceng.2018.02.041

Gao, W., Tang, Q., Ye, B., Yang, Y., & Yao, J. (2020). An enhanced heuristic ant colony optimization for mobile robot path planning. *Soft Computing*, *24*(8), 6139–6150. doi:10.1007/s00500-020-04749-3

Jiao, Z., Ma, K., Rong, Y., Wang, P., Zhang, H., & Wang, S. (2018). A path planning method using adaptive polymorphic ant colony algorithm for smart wheelchairs. *Journal of Computational Science*, *25*, 50–57. doi:10.1016/j.jocs.2018.02.004

Lian, J., Yu, W., Xiao, K., & Liu, W. (2020). Cubic spline interpolation-based robot path planning using a chaotic adaptive particle swarm optimization algorithm. *Mathematical Problems in Engineering*, *2020*, 1–20. Advance online publication. doi:10.1155/2020/1849240

Orozco-Rosas, U., Montiel, O., & Sepúlveda, R. (2019). Mobile robot path planning using membrane evolutionary artificial potential field. *Applied Soft Computing*, *77*, 236–251. doi:10.1016/j.asoc.2019.01.036

Shiling, Z. (2020). Application of joint immune ant colony algorithm and fuzzy neural network to path planning and visual image processing of inspection robot in substation. In *Proceedings of the 2020 3rd International Conference on Artificial Intelligence and Big Data (ICAIBD)* (pp. 142–148). IEEE. doi:10.1109/ICAIBD49809.2020.9137437

Wang, D., Chen, S., Zhang, Y., & Liu, L. (2021). Path planning of mobile robot in dynamic environment: Fuzzy artificial potential field and extensible neural network. *Artificial Life and Robotics*, *26*(1), 129–139. doi:10.1007/s10015-020-00630-6

Wang, H., Li, J., Zhou, Y., Fu, M., & Yang, S. (2019). Research on the technology of indoor and outdoor integration robot inspection in substation. In *Proceedings of the 2019 IEEE 3rd Information Technology, Networking, Electronic and Automation Control Conference (ITNEC)* (pp. 2366–2369). IEEE. doi:10.1109/ITNEC.2019.8729355

Wang, H., Wang, Z., Yu, L., Wang, Q., & Liu, C. (2018). A hybrid algorithm for robot path planning. In *Proceedings of the 2018 IEEE International Conference on Mechatronics and Automation (ICMA)* (pp. 986–990). IEEE. doi:10.1109/ICMA.2018.8484297

Wang, L., Luo, C., Li, M., & Cai, J. (2017). Trajectory planning of an autonomous mobile robot by evolving ant colony system. *International Journal of Robotics and Automation*, *32*(4), 406–413. doi:10.2316/Journal.206.2017.4.206-4917

Wang, T.-M., Tao, Y., & Liu, H. (2018). Current researches and future development trend of intelligent robot: A review. *International Journal of Automation and Computing*, *15*(5), 525–546. doi:10.1007/s11633-018-1115-1

Wang, X.-Y., Yang, L., Zhang, Y., & Meng, S. (2018). Robot path planning based on improved ant colony algorithm with potential field heuristic. *Control and Decision*, *33*(10), 1775–1781. doi:10.13195/j.kzyjc.2017.0639

Zhang, C. (2018). Path planning for robot based on chaotic artificial potential field method. *IOP Conference Series: Materials Science and Engineerin*g, *317*(1), 012056. 10.1088/1757-899X/317/1/012056

Zhang, X., Liu, S., & Xiang, Z. (2019). Optimal Inspection Path planning of substation robot in the complex substation environment. In *Proceedings of the 2019 Chinese Automation Congress (CAC)* (pp. 5064–5068). IEEE. doi:10.1109/CAC48633.2019.8996834

Zhao, J., & Wang, Q. (2022). Design and implementation of an intelligent moving target robot system for shooting training. *International Journal of Information Technologies and Systems Approach*, *16*(2), 1–19. doi:10.4018/IJITSA.320512